JACS
JOURNAL OF THE AMERICAN CHEMICAL SOCIETY
Article
pubs.acs.org/JACS

Accounting for the Dynamic Oxidative Behavior of Nickel Anodes

Rodney D. L. Smith and Curtis P. Berlinguette*

Departments of Chemistry and Chemical & Biological Engineering, The University of British Columbia, 2036 Main Mall, Vancouver, British Columbia V6T1Z1, Canada

Supporting Information

ABSTRACT: The dynamic behavior of the anodic peak for amorphous nickel oxy/hydroxide (a-NiO_x) films in basic media was investigated. Chronocoulometry of films with known nickel concentrations reveals that a total of four electrons per nickel site comprise the signature anodic peak at 1.32 V during the first oxidative scan, and two electrons are passed through the associated cathodic peak on the reverse scan. The anodic and cathodic signals each contain two electrons on the successive scans. Catalytic oxygen evolution reaction (OER) was detected within the anodic peak, which is at a lower potential than is widely assumed. In order to rationalize these experimental results, we propose that the four-electron oxidation event is the conversion of the film from nickel(II) hydroxide ($[Ni^{II}–OH]^-$) to a higher valent nickel peroxide species (e.g., $Ni^{IV}–OO$ or $Ni^{III}–OO\cdot$). The subsequent reduction of the nickel peroxide species is confined by a chemical step resulting in the accumulation of $[Ni^{II}–OOH]^-$, which is then oxidized by two electrons to form $Ni^{IV}–OO$ during the subsequent oxidative scan on the time scale of a cyclic voltammetric experiment. Our proposed mechanism and the experimental determination that each nickel site is oxidized by four electrons helps link the myriad of seemingly disparate literature data related to OER catalysis by nickel electrodes. The faster catalysis that occurs at higher oxidative potentials is derived from a minority species and is not elaborated here.

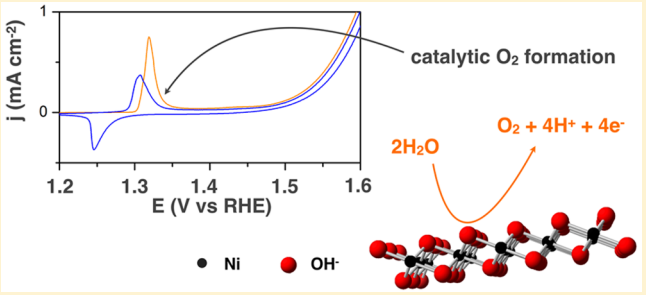

INTRODUCTION

Research efforts over the past several decades have laid the foundation for the models currently used to describe the electrochemistry of nickel oxy/hydroxide films.[1−4] This class of materials serves as the cathode in some battery technologies, and as the anode material in commercial alkaline electrolyzers that catalyze the oxygen evolution reaction (OER; eq 1). The important role that these films play in the energy storage markets provides the imperative to better understand the mechanism by which they operate, thus driving renewed interest in elucidating the redox behavior of this material.[5−13]

$$4OH^- \rightarrow O_2 + 2H_2O + 4e^- \qquad E^o = 0.401\ V \qquad (1)$$

Bode and co-workers established the paradigm of nickel oxy/hydroxide electrochemistry half a century ago by showing that four distinct phases exist (Figure 1).[2] It is widely accepted that two-dimensional sheets of edge-sharing $Ni^{II}(OH)_6$ octahedra, β-$Ni(OH)_2$, are linked by a one-electron transfer step (E_β) to β-Ni(O)OH,[10,14] where both phases are characterized by sharp XRD signals indicating uniform interplanar spacings.[15,16] The other two phases feature relatively disordered axial symmetry, where the reduced α-$Ni(OH)_2$ phase can be converted to γ-Ni(O)OH by the transfer of 1.1−1.8 electrons (E_γ).[17] The four phases are interconvertible: The over oxidation of β-Ni(O)OH can yield γ-Ni(O)OH, and aging of the disordered α/γ phases can lead to the formation of the ordered β phase.[1−4] The α/γ and β/β phases are each characterized by a single, quasi-reversible redox couple in cyclic voltammetric experiments, where E_β is anodically shifted from E_γ.

A tenet of Bode's model is that the electron transfer processes for the β/β and α/γ cycles are different, where the β/β cycle involves a one-electron oxidation of Ni(II) to Ni(III), while the α/γ cycle has been shown to involve a higher-valent nickel site. Coulometric/iodometric studies have shown that the β/β phases are linked by one electron,[8,17] but there are several experimental findings that present the possibility that E_β and E_γ represent the same electrochemical process. Consider that the primary structural difference is thought to be the interlayer spacings between similar covalent networks,[15,16] and that the X-ray photoelectron spectroscopy (XPS) data measured on the two phases is strikingly similar.[18] Moreover, spectroscopic,[17] magnetic,[19] and electrochemical experiments[17] also call into question whether β-$Ni(OH)_2$ is oxidized by merely one electron. These seemingly incoherent experimental outcomes have precluded consensus on the actual number of electrons (1,[10,14,20] ∼ 1.6,[8,17] or more[21]) comprising the oxidation ($E_{p,a}$) and corresponding reduction ($E_{p,c}$) peaks in the cyclic voltammograms (CVs). This lack of clarity is further complicated by the study of films with different thicknesses and morphologies at different pH values,[17] and the sensitivity of the films to infinitesimally small quantities of impurities.[9,22] These

Received: October 21, 2015
Published: February 1, 2016

DOI: 10.1021/jacs.5b10728
J. Am. Chem. Soc. 2016, 138, 1561−1567

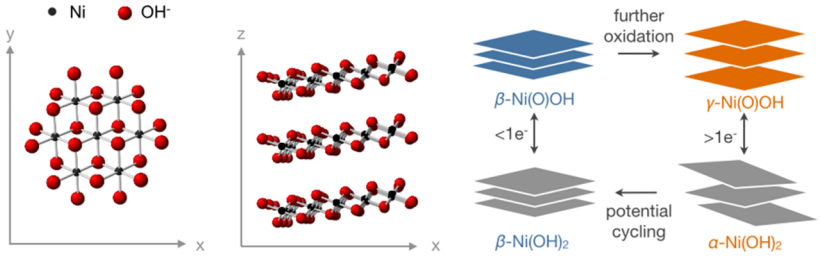

Figure 1. Edge-sharing $Ni(OH)_6$ units comprise stacked sheets of β-$Ni(OH)_2$, which is linked to three other phases that are differentiated by axial interplanar symmetry and redox behavior.

collective factors have led to conflicting views as to how the OER is actually catalyzed by nickel oxy/hydroxides.[7,20]

We report here a different description of the redox chemistry associated with amorphous nickel oxy/hydroxides (a-NiO_x) that unifies the vast majority of data recorded on nickel films, particularly the dynamic electrochemical response of $E_{p,a}$ that has been reported but not previously elaborated.[17] The study of films of a-NiO_x that were not anodized prior to study helped us resolve that the first oxidative scan is distinctively different to those measured during subsequent sweeps. Importantly, the anodic peak measured during the initial oxidative scan ($E_{p,a1}$) at 1.32 V vs the normal hydrogen electrode (NHE) was measured to contain *four* electrons per nickel site, while the subsequent reduction of the oxidized film yields a cathodic peak ($E_{p,c}$) containing two electrons per nickel site; subsequent oxidative and reductive scans produce anodic ($E_{p,a2}$) and cathodic ($E_{p,c}$) peaks that each correspond to the two electrons per nickel site that is more commonly reported. Notably, the four electrons that pass through $E_{p,a1}$ can be regenerated by leaving the electrochemically reduced electrodes to rest in solution for several minutes.

In order to rationalize this dynamic behavior involving four electrons per metal site, we propose that the films follow the catalytic cycle described in Figure 2. This scheme suggests the existence of two distinctive redox processes, where the first oxidative scan captures the redox behavior of $E^{o\prime 1}$ prior to getting locked in a second redox cycle ($E^{o\prime 2}$) on the time scale of a cyclic voltammetry experiment. This proposal implicates catalytic water oxidation when passing through the $E_{p,a}$, which is supported by rotating ring disk electrode (RRDE) experiments. Note that the rate of catalysis is slow until further oxidation of the films triggers a redox event at a minority species that is apparently responsible for the rapid and useful OER electrocatalysis that is more widely investigated. This revised accounting of electrons for $E_{p,a}$ and $E_{p,c}$ has significant implications for assessing nickel-based electrodes.

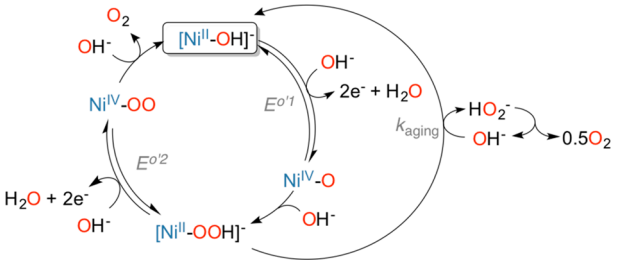

Figure 2. Proposed reaction steps for OER electrocatalysis mediated by a-NiO_x at pH 14 to account for the four electrons being removed from each nickel site. The $[Ni^{II}–OH]^-$ species represents the starting point of the cycle. The higher-valent nickel species merely represent a doubly oxidized species and are not suggestive of the oxygen binding mode, metal–ligand bond order, and relevant resonance forms (e.g., $Ni^{III}–O^{\bullet}$, $Ni^{III}–OO^{\bullet}$).

EXPERIMENTAL SECTION

Materials. Ni(II) 2-ethylhexanoate (78% *w/w* in 2-ethylhexanoic acid) was purchased from Strem Chemicals, $Ni(NO_3)_2{\cdot}6H_2O$ (99.9985%) was purchased from Alfa-Aesar, and KOH, K_2CO_3 and KH_2PO_4 were purchased from Fisher Scientific.

Electrolyte Solutions Preparations. Electrolyte solutions were prepared in the pH 10–14 range by adding appropriate volumes of 30% KOH to solutions containing 0.5 M K_2CO_3 (pK_{a2} = 10.3) and 0.5 M KH_2PO_4 (pK_{a3} = 12.7). A fresh solution was used for electrochemical measurements at each pH value. The pH of each solution was verified before and after use by a Fisher Scientific Accumet AB150 pH meter. Iron impurities were scrubbed from electrolyte solutions that were used for analysis of NiO_x. Following a previously described protocol,[9] $Ni(NO_3)_2{\bullet}6H_2O$ (5.08 g, 0.0175 mol) was dissolved in 12 mL of H_2O prior to addition of 50 mL of 1 M KOH to drive the precipitation of $Ni(OH)_2$. The solid was collected by centrifugation and separated, in equal parts, into one Nalgene bottle containing 150 mL of 30% KOH, and another containing 200 mL of a solution containing 0.5 M K_2CO_3 and 0.5 M KH_2PO_4. Each bottle was sealed and left to stand for 3 days with intermittent agitation to suspend the $Ni(OH)_2$. Appropriate amounts of the purified 30% KOH solutions were added to portions of the purified buffer solution to obtain a range of solutions with pH 10–14, which were verified by a pH meter.

Film Preparation. a-NiO_x films were prepared by a previously reported photochemical procedure[5,6] or anodic electrodeposition.[23] For the photochemical route, a thin film of nickel(II) 2-ethylhexanoate was drop cast onto FTO or gold (0.205 cm^2) from a 0.35 M solution of the metal complex. The coated electrodes were subjected to irradiation by UV light (Atlantic Ultraviolet GPH436T5/VH/HO/4PSE lamp, 185/254 nm) until vibrational modes associated with the ligands were no longer observable by FT-IR spectroscopy.[5] Anodic electrodeposition was performed using an aqueous solution, prepared using iron-free water, containing 0.1 M $NaB(OH)_4$ and 0.4 mM $Ni(NO_3)_2$. a-NiO_x was electrodeposited on the glassy carbon (GC) disk of an RRDE by applying +1.0 V vs. SSCE until the desired charge passed. An approximately linear correlation was observed between charge passed during deposition and the area under $E_{p,a2}$ (Figure S2).

Electrochemistry. Electrochemical data was recorded with a CHI660E potentiostat using a platinum wire counter electrode, Ag/AgCl reference electrode (SSCE), and the appropriate a-NiO_x coated working electrode. The reference electrode was calibrated against RHE by bubbling H_2 gas over a Pt electrode in 1 M KOH. Potentials were not corrected for uncompensated resistance. CVs were acquired at scan rate of 1 mV s^{-1}, unless otherwise indicated. Steady state electrochemical data was acquired by a series of amperometric experiments (60-s intervals, 10 mV steps from 1.07 to 1.67 V vs RHE) on the a-NiO_x coated GC disk of an RRDE electrode that was rotated at 1500 rpm. The platinum ring was held at a constant −0.5 V vs SSCE during the experiments, a potential sufficient to electrochemically reduce O_2 (Figure S5). The potential where i_{Pt} began to increase in magnitude, as determined by the potential where $d\log(-i_{Pt})/dE$ turned

DOI: 10.1021/jacs.5b10728
J. Am. Chem. Soc. 2016, 138, 1561–1567

positive, was taken as the potential where dioxygen was detected (represented as E_{O2} in Figure 5).

Quantification of Nickel in Films. Following electrochemical characterization, an *a*-NiO_x film was dissolved in 2% HNO_3 and diluted to a total volume of 50.00 mL. A 5 mL aliquot of this solution was further diluted to 50 mL. The concentration of nickel in the sample solution was determined by inductively coupled plasma-mass spectrometry (ICP-MS) using a calibration curve generated from seven standard solutions that were prepared using $Ni(NO_3)_2{\cdot}6H_2O$ (99.9985%) in 2% HNO_3 (Figure 4c). An internal standard (^{115}In) was added to the solutions to ensure consistency in injection. A relative standard deviation of 1.0% was measured for the ^{115}In signal intensity for all solutions examined.

Raman Spectroscopy. A 785 nm laser (Innovative Photonic Solutions, 120 mW output power) was focused on an *a*-NiO_x film, deposited on an Au substrate, using an Olympus BX51 microscope (330-μm diameter focus point). A fiber optic bundle transported scattered light to a Princeton Instruments SP2300 spectrograph and a Princeton Instruments PIXIS back-illuminated CCD. *In-situ* spectroelectrochemical data was acquired by mounting an *a*-NiO_x coated Au substrate in a shallow Teflon cell. A Pt wire was employed as a pseudoreference electrode and Ni mesh as the counter electrode. Au substrates were coated with a layer of Au nanoparticles prior to *a*-NiO_x deposition by drop casting a single drop of aqueous Au NP solution (Sigma-Aldrich, 50 nm citrate-stabilized Au particles).

Electrolyte solutions for isotopic labeling studies were prepared by adding 200 μL of 7.4 M KOH to 1.00 g of $H_2{}^{18}O$ (97% ^{18}O, Cambridge Isotope Laboratories, Inc.). With a density of 1.11 g mL^{-1} for $H_2{}^{18}O$, the dilution produces a final solution with ca. 79% $H_2{}^{18}O$.

RESULTS AND DISCUSSION

The films analyzed in this study were prepared, unless otherwise stated, by the photochemically driven decomposition of nickel(II) 2-ethylhexanoate on gold substrates.[5,6] This preparative technique yields thin films of amorphous nickel oxyhydroxide, *a*-NiO_x, which exhibit electrochemical behavior indistinguishable to electrodeposited films common to most literature reports, and provides the opportunity to investigate the films that have not been previously anodized. All electrochemical data herein is reported versus the reversible hydrogen electrode (RHE) and recorded at pH 14, unless otherwise stated, in electrolyte solutions devoid of iron impurities.[9]

CVs acquired on films of *a*-NiO_x at the slow scan rate of 1 mV s^{-1} show a sharp oxidation peak ($E_{p,a1}$) at 1.32 V prior to a spike in current (E_a) at *ca.* 1.47 V that is a signature of rapid OER catalysis (Figure 3). The return scan produces a cathodic peak, $E_{p,c}$, at 1.25 V. The second cycle reveals a cathodically shifted oxidative peak, $E_{p,a2}$, centered at 1.31 V characterized by a peak current density approximately half that of $E_{p,a1}$, while the E_a and $E_{p,c}$ values and profiles were the same as those measured in the first cycle. Subsequent and continuous cycling of *a*-NiO_x yielded traces superimposable with the scan recorded on the second cycle.

The electrodes subjected to electrochemical conditioning could be converted back to the same phase as the fresh electrode (*i.e.*, films characterized by $E_{p,a1}$) by resting at open-circuit (V_{oc}) in the electrolyte solution for >20 min. The $E_{p,a1}$ signal measured on the regenerated films was again shifted back to $E_{p,a2}$ after the first oxidative scan. This dynamic electrochemical behavior persists over the 10−14 pH range for photochemically deposited *a*-NiO_x films (Figure 3b). All redox features ($E_{p,a1}$, $E_{p,a2}$, E_a, and $E_{p,c}$) exhibit a *ca.* 90 mV pH^{-1} dependence on pH, similar to that previously reported for electrodeposited *a*-NiO_x,[7] yielding a ∼30-mV pH^{-1} anodic shift relative to the RHE scale (Figure 3b). The dynamic

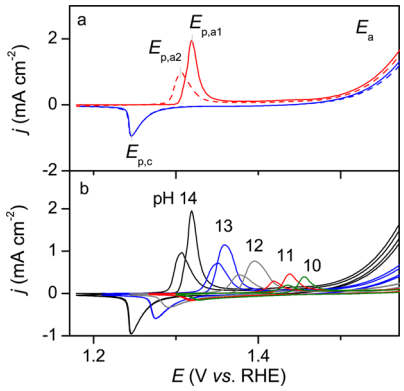

Figure 3. (a) CVs recorded on *a*-NiO_x highlighting the dynamic behavior between the initial anodic sweep (solid red) and all subsequent anodic sweeps (dashed red); all cathodic sweeps (blue) are uniform. (b) CVs recorded on *a*-NiO_x over the pH 10−14 range. The *a*-NiO_x film was held at *ca.* 0.9 V vs RHE for 20 min in each buffer solution, which regenerated the dynamic electrochemical behavior. All experiments were performed at 1 mV s^{-1} on *a*-NiO_x photodeposited on an Au substrate.

electrochemical behavior reported here was confirmed at pH 14 for *a*-NiO_x prepared by alternative electrodeposition method (Figure S1) on a variety of substrates (glassy carbon, fluorine−tin oxide, gold). These results demonstrate the reproducible chemical reversibility of this phase transition.

A potential-step protocol was followed to quantify the relative charge passed through the oxidative ($E_{p,a1}$ and $E_{p,a2}$) and reductive ($E_{p,c}$) peaks during successive oxidation and reduction cycling of the films over the 1.17−1.47 V range (Figure 4a). The ratio of anodic charge, Q_a, to cathodic charge, Q_c, passed during the initial oxidation and subsequent reduction of *a*-NiO_x was measured to be ∼1.9, with a marked decrease to ∼1.3 upon successive cycling. Leaving the electrode rest in the electrolyte solution for 20 min before resuming this potential-step protocol yielded a Q_a/Q_c ratio of 2.1, confirming that the phase of the experienced film could be converted back to that of the original film. These electrochemical experiments were repeated on a fresh electrode (Figure 4b) prior to dissolution of the film in 2% HNO_3 for the quantification of the nickel concentration by inductively coupled plasma-mass spectrometry (ICP-MS; Figure 4c) to quantify the number of electrons per nickel site in the films (Figure 4d). This protocol indicated that the oxidation of the fresh electrode ($E_{p,a1}$) involved the transfer of ∼4.1 electrons per nickel site, with 1.7 electrons per nickel site being measured for the subsequent reductive process (Figure 4d). In contrast, the second oxidation cycle was measured to have only 2.0 electrons per nickel atom within $E_{p,a2}$, with 1.6 electrons per metal site comprising $E_{p,c}$. Successive cycling produced a gradual decrease in both the oxidation and reduction processes that converged on values of 1.5 and 1.3 electrons for $E_{p,a2}$ and $E_{p,c}$, respectively, for the 10th cycle. The ∼1.6 electrons that comprise the $E_{p,c}$ signal are in excellent agreement with literature reports,[8,17] lending credence to the measured value of four electrons per nickel site comprising the $E_{p,a1}$ peak.

Steady-state current density (j_{NiOx}) measurements were performed on *a*-NiO_x films over a potential window that fully encompassed $E_{p,a}$ to better understand the dynamic voltammetric behavior. Three distinct steady-state current regions were observed (Figure 5a): (**I**) Constant j_{NiOx} up to ∼ 1.27 V; (**II**) constant but higher j_{NiOx} from ∼1.27 to 1.42 V; and (**III**) a

DOI: 10.1021/jacs.5b10728
J. Am. Chem. Soc. 2016, 138, 1561−1567

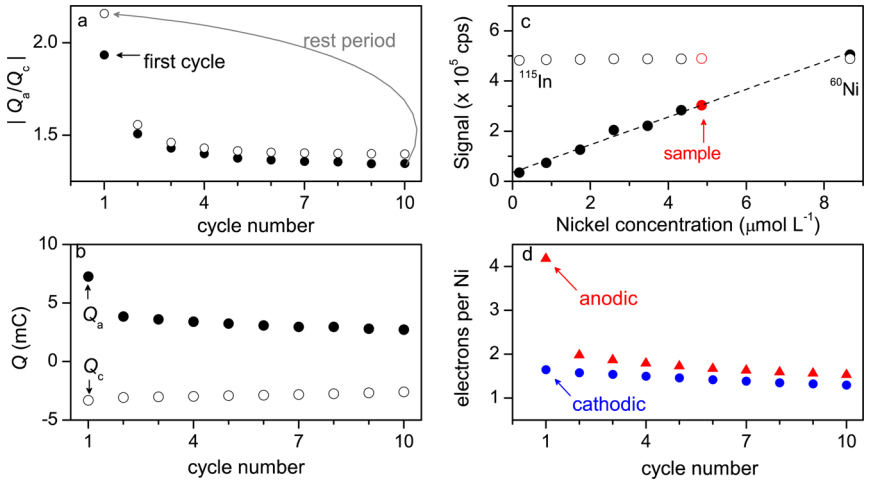

Figure 4. (a) Q_a/Q_c ratio for a fresh *a*-NiO_x electrode (solid circles), and on the experienced film after resting in solution at open-circuit for 20 min (hollow circles), highlighting the ability to reproducibly chemically regenerate the dynamic electrochemical behavior. (b) The anodic (Q_a) and cathodic (Q_c) charge required to fully oxidize/reduce an *a*-NiO_x film was determined by performing 60-s potential steps between 1.47 and 1.17 V vs. RHE. (c) The *a*-NiO_x film was subsequently dissolved in 2% HNO_3, and the nickel content of the solution was determined using ICP-MS and calibrated against freshly prepared standard solutions (black circles). An internal standard was used to confirm injection consistency for all samples (^{115}In, hollow circles). (d) The number of electrons transferred per nickel atom was calculated by comparison of the anodic (1.47 V, red triangles) and cathodic (1.17 V, blue circles) charges passed during potential step experiments with the ICP-MS results. All electrochemical experiments were performed on photochemically deposited *a*-NiO_x on a gold substrate at pH 14.

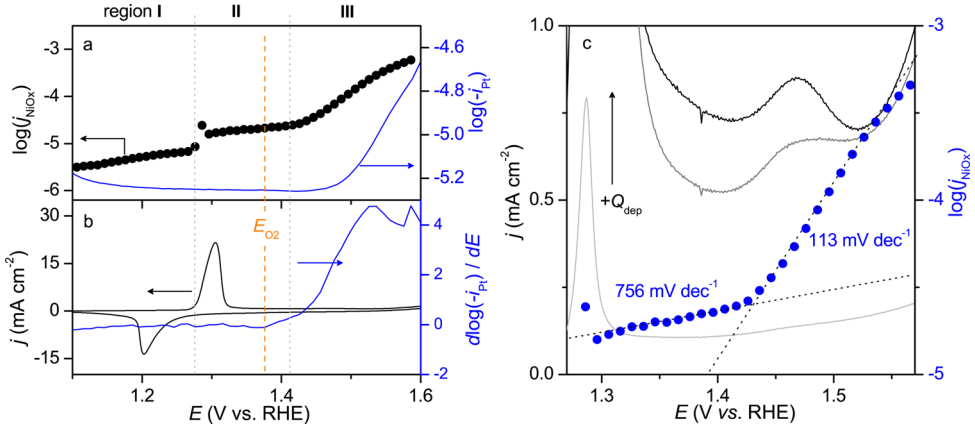

Figure 5. (a) Steady-state current density recorded on an *a*-NiO_x-coated glassy carbon disk (prepared by 5-mC anodic electrodeposition) measured by potential-step experiments (60-s intervals in 10 mV steps) using a RRDE while dioxygen evolution was monitored by the platinum ring. (b) CV acquired at 1 mV s^{-1} on the same electrode and the derivative plot used to determine the point at which dioxygen was detected (vertical orange line). Regions **I**–**III** represent the different regimes as described in the text. (c) Anodic potential sweeps (100 mV s^{-1}) on electrodeposited *a*-NiO_x (Q_{dep} = 0.5, 3.0, and 5.0 mC) show the emergence of an oxidation peak at higher Q_{dep}. The location of this peak corresponds to the potential where a change in Tafel slope is observed in the overlaid steady-state current measurements.

marked exponential rise in j_{NiOx} at >1.42 V. The step in $\log(j_{NiOx})$ when transitioning from region **I** to **II** signifies a sustained increase in electron flow at $E_{p,a}$ consistent with an electrocatalytic reaction and not merely a redox process. The transition from region **II** to **III** is characterized by a much faster increase in electron flow, and also a change in Tafel slope to 113 mV dec^{-1}. Rotating ring-disk electrode (RRDE) experiments on thin films of electrodeposited *a*-NiO_x confirmed oxygen evolution in region **III** (Figure S2). Increasing the amount of charge passed to electrodeposit the *a*-NiO_x films (Q_{dep}) shifted the potential cathodically, at which point dioxygen evolution (E_{O2}) was detected by the platinum ring according to $d\log(-i_{Pt})/dE$ vs E plots. Increasing Q_{dep} from 0.5 to 7 mC shifted E_{O2} from 1.45 to 1.38 V, providing direct evidence that the stepwise increase in $\log(j_{NiOx})$ during the transition from region **I** to **II** corresponds to dioxygen evolution. Importantly, our examination of thicker films revealed that the transition from region **II** to **III** is coincident with a small oxidation peak (Figure 5c). We tentatively assign the transition from region **II** to **III** to the engagement of a different reaction site (e.g., an edge site) that is capable of mediating much faster catalysis, but this feature was not investigated further and the mechanism of OER catalysis in region **III** is not indicated in this manuscript.

In order to link this collection of data that is suggestive of a different electron count and earlier onset of catalysis, we suggest the possibility that OER catalysis follows the pathway described in Figure 2. The *a*-NiO_x is presumed to exist as Ni^{II} sheets linked by μ_3–OH^- ligands.[8,13] These sheets are measured to have a pK_a of ~12,[7] and thus we indicate the starting point of the cycle as $[Ni^{II}–OH]^-$ at pH 14 (Figure 2). Our proposal implicates an initial two-electron oxidation to

DOI: 10.1021/jacs.5b10728
J. Am. Chem. Soc. 2016, 138, 1561–1567

convert $[Ni^{II}-OH]^-$ to $Ni^{IV}-O$ (denoted by $E^{o\prime 1}$ in Figure 2) that reacts with OH^- to form $[Ni^{II}-OOH]^-$. This species then proceeds through a second two-electron oxidation process to furnish $Ni^{IV}-OO$ (denoted by $E^{o\prime 2}$ in Figure 2). Subsequent cycling is then restricted to the two-electron conversion between $[Ni^{II}-OOH]^-$ and $Ni^{IV}-OO$ ($E^{o\prime 2}$) on the time scale of a cyclic voltammetry experiment. We emphasize that the high-valent metal species $Ni^{IV}-O$ and $Ni^{IV}-OO$ indicated in Figure 2 can exist as the valence resonance forms $Ni^{III}-O^{\bullet}$ and $Ni^{III}-OO^{\bullet}$, respectively;[18,24−29] the nomenclature we use in Figure 2 is merely for electron counting and is not intended to assign formal oxidation states of the metal. The measurement of 4.1 electrons per nickel atom for $E_{p,a1}$ indicates the accumulation of $Ni^{IV}-OO$ immediately upon oxidation of *a*-NiO_x, suggesting that electrocatalytic OER occurs at $E_{p,a1}$ and at a potential below what is typically considered for nickel electrodes. Electrocatalytic processes are more commonly presented as a sharp rise in current (*e.g.*, region **III** in Figure 5a), but the measured quasi-infinite Tafel slope for region **II** is consistent with the accumulation of an intermediate that precedes a chemical rate-determining step (RDS).[30−33] This feature, in tandem with the detection of dioxygen at potentials within region **II**, supports our assertion of electrocatalysis at the lower potentials.

Given that our proposal implicates the buildup of a peroxide species, Raman spectra were recorded on photodeposited *a*-NiO_x films while held at 1.4 V to test whether nickel-peroxo or nickel-superoxo species at 800−950 cm^{-1} and 971−1131 cm^{-1}, respectively, were present.[34−40] Spectral signals for the oxidized (480 and 559 cm^{-1}) and reduced (465 cm^{-1}) films were consistent with Ni−O vibrational modes (Figure S3a).[14,41−45] A weak, asymmetric feature at 1067 cm^{-1} measured for the oxidized films is consistent with a nickel-peroxo/superoxo species (Figure S3a, inset), which is validated by the shift to 1044 cm^{-1} when recorded in enriched $H_2{}^{18}O$ (a 30 cm^{-1} difference is expected for $^{16}O-^{16}O$ and $^{16}O-^{18}O$ modes; Figure S3c). Visible gas evolution was triggered by the laser irradiation required for the Raman experiments when *a*-NiO_x was held at 1.4 V vs. RHE, presumably due to dioxygen evolution. While this signal was not present for the electrochemically reduced films with >5-s laser pulses, 2-s laser pulses facilitated the emergence of an $\sim$ 850 cm^{-1} signal and diminution of the 1067 cm^{-1} signal (Figure S3b). Raman (and inelastic neutron scattering) signals at 800 to 1100 cm^{-1} have been previously documented for oxidized $Ni(OH)_2$ and attributed to the oscillation of free protons within the crystal lattice, Ni−O, or second harmonic vibrations.[21,41,43−45] Some of these features are not expected in a disordered amorphous film, but we cannot completely rule out second order effects rather than the high intensity of the laser decomposing the film. While the weak spectral signals are unsatisfying for a film that we purport to have an abundance of peroxide, recent independent reports have documented spectral signals in this same region attributed to an "active oxygen" or peroxide species,[21,46] lending further support to our proposal that a nickel-peroxide species precedes the RDS step.

The biphasic two-electron chemistry represented by $E^{o\prime 1}$ and $E^{o\prime 2}$ is also supported by the successive scans in the CV experiments that show four and two electrons per nickel site for $E_{p,a1}$ and $E_{p,a2}$, respectively. The measurement of four electrons per nickel site during the initial oxidation of *a*-NiO_x (Figure 4) indicates that both electron transfer phases $E^{o\prime 1}$ and $E^{o\prime 2}$ occur at approximately the same potential during the first oxidation cycle, and that O−O bond formation occurs faster than dioxygen release. Our assignment of the RDS following the $Ni^{IV}-OO$ species rather than the $Ni^{IV}-O$ is not one that we initially considered, but we are unable to provide an alternative explanation that explains how four electrons can be removed from each nickel site. Our proposal is nonetheless aligned with the entire body of electrochemical data provided here, and the spectroscopic evidence of a peroxo species in our experiments and others.[21,46] It is also important to note that our proposal is also directly aligned with the catalytic cycles that have been unambiguously elucidated for homogeneous single-site catalysts, some of which have a RDS that is assigned to dixoygen evolution rather than dioxygen formation.[47,48] Our proposal also implicates catalysis at bulk metal sites and not exclusively at edge sites. While this possibility may seem remote, the exceedingly slow rate of catalysis ($\tau_{1/2} \sim 2$ h) in regime **II** would enable the recovery of the lattice oxygen atom displaced during catalysis prior to the decomposition of the covalent network.

The shift in $E_{p,a}$ that is observed between the first and second cycles in Figure 3a suggests that $E^{o\prime 1}$ is more anodic than $E^{o\prime 2}$. The oxidation and reduction peaks for the successive cycles consisting of *ca.* two electrons per nickel site arise from the irreversible O−O bond formation step precluding electrochemical reduction of $[Ni^{II}-OOH]^-$ to $[Ni^{II}-OH]^-$ on the time scale of the CV experiment. Consequently, the second scan in the CV represents oxidation of accumulated $[Ni^{II}-OOH]^-$ and not $[Ni^{II}-OH]^-$, thus, $E_{p,c}$ and $E_{p,a2}$ are presented as a two-electron event ($E^{o\prime 2}$). The inability to electrochemically regenerate the behavior of the electrodes on the time scale of the CV experiments supports the notion that a chemical step (k_{aging}) provides access to the original phase of the film. Further support for our mechanism is provided by slow catalytic water oxidation at 1.32 V, revealed by the detection of dioxygen and steady-state experiments on a RDDE, and an infinite Tafel slope. CVs obtained at variable scan rates show a significant broadening and shift for both $E_{p,a2}$ and $E_{p,c}$ (Figure S4a), along with a diminished amount of charge passed (Figure S4b), when the scan rate was increased above ~5 mV s^{-1}. These results indicate that a slow process exerts significant influence on the electrochemical behavior. Examining the films at slow scan rates is therefore crucial: rates >1 mV s^{-1} that are commonly reported may result in incomplete oxidation of the film.

CONCLUSIONS

The dynamic behavior of the $E_{p,a}$ signal when NiO_x is measured in strongly basic media is known but rarely addressed. Indeed, many reports do not show the first scan of a cyclic voltammogram recorded on *a*-NiO_x and report only the data on the conditioned electrodes. This work shows that the change in peak position and size of $E_{p,a}$ may arise from four electrons per metal site being transferred during the initial oxidation of the film prior to confinement within a two-electron redox cycle. Our data also provides compelling evidence that electrocatalytic OER commences immediately upon oxidation of *a*-NiO_x (regime **II**, Figure 5), albeit very slowly. Faster catalysis (regime **III**, Figure 5) does not occur until another redox event at smaller number of active sites at higher potentials.

We propose a mechanism for electrocatalytic OER in regime **II** that is aligned with that of homogeneous catalysts containing a single metal center.[47,48] Our mechanism accounts for: (i) dynamic electrochemical behavior during potential cycling, (ii)

DOI: 10.1021/jacs.5b10728
J. Am. Chem. Soc. 2016, 138, 1561−1567

passive regeneration of this dynamic behavior by merely leaving the electrode in electrolyte solution at open-circuit; (iii) a chemical RDS (e.g., dioxygen release); (iv) Raman spectroscopy indicating a peroxide species under steady-state conditions; (v) RRDE experiments indicating dioxygen evolution within regime **II**; and (vi) independently collected XAS measurements showing a high-valent nickel site.[8] We are currently unable to reconcile the four-electron oxidation of each nickel site with a rate-limiting O−O bond formation step, and therefore assign the RDS to the liberation of dioxygen in order to conform to our entire collection of data. This proposal raises the possibility that researchers may be unwittingly measuring the oxidative behavior of $[Ni^{II}-OOH]^-$ rather than $[Ni^{II}-OH]^-$. Further studies are underway to validate this hypothesis.

■ ASSOCIATED CONTENT

Supporting Information

The Supporting Information is available free of charge on the ACS Publications website at DOI: 10.1021/jacs.5b10728.

Supplementary Discussion and CVs, plots of amount of charge, Raman spectra, and rotating ring disk experiments (PDF)

■ AUTHOR INFORMATION

Corresponding Author

*cberling@chem.ubc.ca

Notes

The authors declare no competing financial interest.

■ ACKNOWLEDGMENTS

University of British Columbia (UBC) start-up funds and Canada Research Chairs are recognized for their financial support. This research used facilities funded by UBC and the Canadian Foundation for Innovation. We also thank Prof. Edward Grant for access to a Raman spectrometer. Finally, we are also grateful for the valuable input provided by several reviewers of this manuscript.

■ REFERENCES

(1) Doyle, R. L.; Godwin, I. J.; Brandon, M. P.; Lyons, M. E. G. *Phys. Chem. Chem. Phys.* **2013**, *15*, 13737−13783.
(2) Bode, H.; Dehmelt, K.; Witte, J. *Electrochim. Acta* **1966**, *11*, 1079−1087.
(3) Oliva, P.; Leonardi, J.; Laurent, J. F.; Delmas, C.; Braconnier, J. J.; Figlarz, M.; Fievet, F.; de Guibert, A. *J. Power Sources* **1982**, *8*, 229−255.
(4) Rebouillat, S.; Lyons, M. E. G.; Brandon, M. P.; Doyle, R. L. *Int. J. Electrochem. Sci.* **2011**, *6*, 5830−5917.
(5) Smith, R. D. L.; Prevot, M.; Fagan, R. D.; Zhang, Z.; Sedach, P. A.; Siu, M. K. J.; Trudel, S.; Berlinguette, C. P. *Science* **2013**, *340*, 60−63.
(6) Smith, R. D. L.; Prevot, M.; Fagan, R. D.; Trudel, S.; Berlinguette, C. P. *J. Am. Chem. Soc.* **2013**, *135*, 11580−11586.
(7) Bediako, D. K.; Surendranath, Y.; Nocera, D. G. *J. Am. Chem. Soc.* **2013**, *135*, 3662−3674.
(8) Bediako, D. K.; Lassalle-Kaiser, B.; Surendranath, Y.; Yano, J.; Yachandra, V. K.; Nocera, D. G. *J. Am. Chem. Soc.* **2012**, *134*, 6801−6809.
(9) Trotochaud, L.; Young, S. L.; Ranney, J. K.; Boettcher, S. W. *J. Am. Chem. Soc.* **2014**, *136*, 6744−6753.
(10) Louie, M. W.; Bell, A. T. *J. Am. Chem. Soc.* **2013**, *135*, 12329−12337.
(11) Friebel, D.; Louie, M. W.; Bajdich, M.; Sanwald, K. E.; Cai, Y.; Wise, A. M.; Cheng, M.-J.; Sokaras, D.; Weng, T.-C.; Alonso-Mori, R.; Davis, R. C.; Bargar, J. R.; Nørskov, J. K.; Nilsson, A.; Bell, A. T. *J. Am. Chem. Soc.* **2015**, *137*, 1305−1313.
(12) Klaus, S.; Cai, Y.; Louie, M. W.; Trotochaud, L.; Bell, A. T. *J. Phys. Chem. C* **2015**, *119*, 7243−7254.
(13) Risch, M.; Klingan, K.; Heidkamp, J.; Ehrenberg, D.; Chernev, P.; Zaharieva, I.; Dau, H. *Chem. Commun.* **2011**, *47*, 11912−11914.
(14) Yeo, B. S.; Bell, A. T. *J. Phys. Chem. C* **2012**, *116*, 8394−8400.
(15) Mani, B.; de Neufville, J. P. *J. Electrochem. Soc.* **1988**, *135*, 800−803.
(16) Wehrens-Dijksma, M.; Notten, P. H. L. *Electrochim. Acta* **2006**, *51*, 3609−3621.
(17) Corrigan, D. A.; Knight, S. A. *J. Electrochem. Soc.* **1989**, *136*, 613−619.
(18) Biesinger, M. C.; Payne, B. P.; Lau, L. W. M.; Gerson, A.; Smart, R. S. C. *Surf. Interface Anal.* **2009**, *41*, 324−332.
(19) Labat, J. *Ann. Chim.* **1964**, *9*, 399−427.
(20) Lyons, M. E. G.; Doyle, R. L.; Godwin, I.; O'Brien, M.; Russell, L. *J. Electrochem. Soc.* **2012**, *159*, H932−H944.
(21) Merrill, M.; Worsley, M.; Wittstock, A.; Biener, J.; Stadermann, M. *J. Electroanal. Chem.* **2014**, *717−718*, 177−188.
(22) Corrigan, D. A. *J. Electrochem. Soc.* **1987**, *134*, 377−384.
(23) Dincă, M.; Surendranath, Y.; Nocera, D. G. *Proc. Natl. Acad. Sci. U. S. A.* **2010**, *107*, 10337−10341.
(24) Gottschall, R.; Schollhorn, R.; Muhler, M.; Jansen, N.; Walcher, D.; Gutlich, P. *Inorg. Chem.* **1998**, *37*, 1513−1518.
(25) van Elp, J.; Eskes, H.; Kuiper, P.; Sawatzky, G. A. *Phys. Rev. B: Condens. Matter Mater. Phys.* **1992**, *45*, 1612−1622.
(26) Grosvenor, A. P.; Biesinger, M. C.; Smart, R. S. C.; McIntyre, N. S. *Surf. Sci.* **2006**, *600*, 1771−1779.
(27) Crandell, D. W.; Ghosh, S.; Berlinguette, C. P.; Baik, M.-H. *ChemSusChem* **2015**, *8*, 844−852.
(28) Yang, X.; Baik, M.-H. *J. Am. Chem. Soc.* **2004**, *126*, 13222−13223.
(29) Moonshiram, D.; Alperovich, I.; Concepcion, J. J.; Meyer, T. J.; Pushkar, Y. *Proc. Natl. Acad. Sci. U. S. A.* **2013**, *110*, 3765−3770.
(30) Bockris, J. O.; Otagawa, T. *J. Phys. Chem.* **1983**, *87*, 2960−2971.
(31) Guidelli, R.; Compton, R. G.; Feliu, J. M.; Gileadi, E.; Lipkowski, J.; Schmickler, W.; Trasatti, S. *Pure Appl. Chem.* **2014**, *86*, 259−262.
(32) Guidelli, R.; Compton, R. G.; Feliu, J. M.; Gileadi, E.; Lipkowski, J.; Schmickler, W.; Trasatti, S. *Pure Appl. Chem.* **2014**, *86*, 245−258.
(33) Lyons, M. E. G.; Doyle, R. L.; Fernandez, D.; Godwin, I. J.; Browne, M. P.; Rovetta, A. *Electrochem. Commun.* **2014**, *45*, 56−59.
(34) Perivolaris, A.; Stoumpos, C. C.; Karpinska, J.; Ryder, A. G.; Frost, J. M.; Mason, K.; Prescimone, A.; Slawin, A. M. Z.; Kessler, V. G.; Mathieson, J. S.; Cronin, L.; Brechin, E. K.; Papaefstathiou, G. S. *Inorg. Chem. Front.* **2014**, *1*, 487−494.
(35) Cho, J.; Furutachi, H.; Fujinami, S.; Tosha, T.; Ohtsu, H.; Ikeda, O.; Suzuki, A.; Nomura, M.; Uruga, T.; Tanida, H.; Kawai, T.; Tanaka, K.; Kitagawa, T.; Suzuki, M. *Inorg. Chem.* **2006**, *45*, 2873−2885.
(36) Brown, E. J.; Duhme-Klair, A.-K.; Elliott, M. I.; Thomas-Oates, J. E.; Timmins, P. L.; Walton, P. H. *Angew. Chem., Int. Ed.* **2005**, *44*, 1392−1395.
(37) Yao, S.; Bill, E.; Milsmann, C.; Wieghardt, K.; Driess, M. *Angew. Chem., Int. Ed.* **2008**, *47*, 7110−7113.
(38) Cho, J.; Sarangi, R.; Annaraj, J.; Kim, S. Y.; Kubo, M.; Ogura, T.; Solomon, E. I.; Nam, W. *Nat. Chem.* **2009**, *1*, 568−572.
(39) Kieber-Emmons, M. T.; Annaraj, J.; Seo, M. S.; Van Heuvelen, K. M.; Tosha, T.; Kitagawa, T.; Brunold, T. C.; Nam, W.; Riordan, C. G. *J. Am. Chem. Soc.* **2006**, *128*, 14230−14231.
(40) Shiren, K.; Ogo, S.; Fujinami, S.; Hayashi, H.; Suzuki, M.; Uehara, A.; Watanabe, Y.; Moro-oka, Y. *J. Am. Chem. Soc.* **2000**, *122*, 254−262.
(41) Bantignies, J. L.; Deabate, S.; Righi, A.; Rols, S.; Hermet, P.; Sauvajol, J. L.; Henn, F. *J. Phys. Chem. C* **2008**, *112*, 2193−2201.
(42) Gourrier, L.; Deabate, S.; Michel, T.; Paillet, M.; Hermet, P.; Bantignies, J.-L.; Henn, F. *J. Phys. Chem. C* **2011**, *115*, 15067−15074.

DOI: 10.1021/jacs.5b10728
J. Am. Chem. Soc. 2016, 138, 1561−1567

(43) Hall, D. S.; Lockwood, D. J.; Poirier, S.; Bock, C.; MacDougall, B. R. *ACS Appl. Mater. Interfaces* **2014**, *6*, 3141−3149.
(44) Hermet, P.; Gourrier, L.; Bantignies, J. L.; Ravot, D.; Michel, T.; Deabate, S.; Boulet, P.; Henn, F. *Phys. Rev. B: Condens. Matter Mater. Phys.* **2011**, *84*, 235211.
(45) Hall, D. S.; Lockwood, D. J.; Poirier, S.; Bock, C.; MacDougall, B. R. *J. Phys. Chem. A* **2012**, *116*, 6771−6784.
(46) Trześniewski, B. J.; Diaz-Morales, O.; Vermaas, D. A.; Longo, A.; Bras, W.; Koper, M. T. M.; Smith, W. A. *J. Am. Chem. Soc.* **2015**, *137*, 15112−15121.
(47) Wasylenko, D. J.; Ganesamoorthy, C.; Henderson, M. A.; Koivisto, B. D.; Osthoff, H. D.; Berlinguette, C. P. *J. Am. Chem. Soc.* **2010**, *132*, 16094−16106.
(48) Concepcion, J. J.; Jurss, J. W.; Templeton, J. L.; Meyer, T. J. *J. Am. Chem. Soc.* **2008**, *130*, 16462−16463.

DOI: 10.1021/jacs.5b10728
J. Am. Chem. Soc. 2016, 138, 1561−1567